New Physics: Sae Mulli,
Vol. 64, No. 7, July 2014, pp. 696∼703
DOI: 10.3938/NPSM.64.696

Effects of Excessive Bi on the Structure and the Properties of Aurivillius $Bi_{5.25}La_{0.75}Fe_2Ti_3O_{18}$ Thin Films

Chinnambedu Murugesan RAGHAVAN · Jin Won KIM · Ji Ya CHOI · Sang Su KIM*
Department of Physics, Changwon National University, Changwon 641-773, Korea

Jong-Woo KIM
Functional Ceramics Group, Korea Institute of Materials Science, Changwon 641-831, Korea

(Received 17 April 2014 : revised 15 May 2014 : accepted 15 May 2014)

The effects of excessive Bi on the structural, electrical and multiferroic properties of the La-doped $Bi_6Fe_2Ti_3O_{18}$ ($Bi_{5.25}La_{0.75}Fe_2Ti_3O_{18}$) thin films prepared on Pt(111)/Ti/SiO_2/Si(100) substrates by using a chemical solution deposition method are reported. The structures of the thin films were studied by using X-ray diffraction, Raman scattering spectroscopy and scanning electron microscopy. From the experimental comparisons, a low electrical leakage current of 1.84×10^{-5} A/cm^2 at 100 kV/cm and enhanced ferroelectric properties, such as a large remnant polarization ($2P_r$) of 10.5 μC/cm^2 and a low coercive field ($2E_c$) of 400 kV/cm at 485 kV/cm, were observed for the 5% Bi-excess La-doped $Bi_6Fe_2Ti_3O_{18}$ thin film. The formation of a stable bismuth layer-structured phase, a lower *c*-axis orientation, an optimum crystallinity and a dense microstructure with a smooth surface morphology correlate with the improved electrical and multiferroic properties of the 5% Bi-excessive $Bi_6Fe_2Ti_3O_{18}$ thin film.

PACS numbers: 77.84.-s, 85.50.Gk
Keywords: Aurivillius La doped $Bi_6Fe_2Ti_3O_{18}$ thin film, Chemical solution deposition, Structure, Multiferroic properties

I. INTRODUCTION

The bismuth layer-structured ferroelectrics (BLSFs) are of recent interest for their unique crystal structure, ferroelectricity with good fatigue endurance, high Curie temperature and lead free nature [1]. The BLSFs were extensively investigated for integrated devices, such as nonvolatile ferroelectric random access memories (NVFeRAMs) [2]. The crystal structures of BLSFs are generally composed by the sandwiching of perovskite like $(A_{n-1}B_nO_{3n+1})^{2-}$ slabs between fluorite like bismuth-oxygen $(Bi_2O_2)^{2+}$ layers [3]. In the above formula A represents mono-, di-, and trivalent ions, B represents tetra-, penta- and hexavalent ions, and n is the number of sheets of corner sharing with BO_6 octahedra in the perovskite blocks [3–5]. In BLSFs, the ferroelectricity mainly originates from the BO_6 octahedra [6]. By changing the number of perovskite layers, the microstructural and physical properties of the materials can be altered significantly [1,7]. Some of the well-known examples for BLSFs series are Bi_2MoO_6 (n =1), $SrBi_2Ta_2O_9$ (n = 2), $Bi_4Ti_3O_{12}$ (n = 3) and $SrBi_4Ti_4O_{15}$ (n = 4) [3]. Among these, the $Bi_4Ti_3O_{12}$ were widely studied for the NVFeRAMs applications due to its large spontaneous polarization and ferroelectric transition temperature [3].

The combination of $Bi_4Ti_3O_{12}$ with a well-known ferroelectric bismuth ferrite ($BiFeO_3$) forms novel BLSFs structures with general formula of $Bi_{n+1}Fe_{n-3}Ti_3O_{3n+3}$ (n = 4, 5, 6, 7, 8, and *etc.*), which are of recent interest for the multiferroic applications [7–14]. Among these series, the $Bi_6Fe_2Ti_3O_{18}$ (n = 5) is considered as much interesting owing to its quadratic magnetoelectric nature [8,11,15–18]. The $Bi_6Fe_2Ti_3O_{18}$ exhibits stable structure with high ferroelctric Curie (∼1075 K) and Neel (∼160

*E-mail: sskim@changwon.ac.kr

K) transition temperatures [8,18]. According to the reports, the $Bi_6Fe_2Ti_3O_{18}$ shows weak antiferromagnetic interaction with dominant paramagnetic state [13]. Recently, the coexistence of ferroelectric and ferromagnetic properties was measured for the Co doped $Bi_6Fe_2Ti_3O_{18}$ sample [17]. In BLSFs, the formation of oxygen vacancies and secondary phases have strong influences on the electrical, piezoelectric, and multiferroic properties of the thin films [19, 20]. The formations of oxygen vacancies and secondary phases in the BLSFs are mainly attributed to the volatilization of high vapor pressure Bi^{3+} ion [20]. In the Bi based ferroelectric compounds, the volatilization of the Bi ion were compensated by a rare earth (*RE*) metal ions substitution [21]. Particularly, the La ion doping is more beneficial for the improvement of electrical and magnetic properties of the BLSFs [11,21,22]. However, to achieve the maximum compensation of Bi volatilization, it is necessary to add excessive Bi into the BLSFs [23]. There are no reports on the effects of excessive Bi on the compensation of Bi volatilization in the *RE* doped $Bi_6Fe_2Ti_3O_{18}$ thin film.

In this investigation, an attempt was made on the compensation of bismuth volatility in *RE* lanthanum(La)-doped $Bi_6Fe_2Ti_3O_{18}$ ($Bi_{5.25}La_{0.75}Fe_2Ti_3O_{18}$, here onwards it has been represented as BLFT) by the addition of excessive Bi ion. The concentration of the excessive Bi ion was varied systematically, 0% (B0LFT), 5% (B5LFT), 10% (B10LFT), 15% (B15LFT) and 20% (B20LFT). The structural, electrical, ferroelectric, and magnetic properties of the thin films were investigated to observe the optimized film quality.

II. EXPERIMENTAL PROCEDURE

The chemicals used for the preparation of precursor solutions are bismuth nitrate pentahydrate ($Bi(NO_3)_3 \cdot 5H_2O$), iron nitrate nonahydrate ($Fe(NO_3)_3 \cdot 9H_2O$), lanthanum nitrate hexahydrate ($La(NO_3)_3 \cdot 6H_2O$) and titanium isopropoxide ($Ti(OCH(CH_3)_2)_4$). A mixture of ethylene glycol ($OH(CH_2)_2OH$) and 2-methoxyethanol (2-MOE) ($CH_3O(CH_2)_2OH$) prepared by constant stirring for 30 min at room temperature was used as a solvent. To the above solvent, acetic acid (CH_3COOH) was added as a catalyst to maintain the viscosity of the solution. Bismuth nitrate pentahydrate (0%, 5%, 10%, 15% and 20% excess), lanthanum nitrate hexahydrate and iron nitrate nonahydrate were added sequentially to the mixed solvent containing a catalyst with 30 min stirring intervals. Separately, 2-MOE and acetylacetone ($CH_3COCH_2COCH_3$) were mixed at room temperature in a glove box for 30 min to make a homogeneous solution. Acetylacetone was used as a chelating agent. Titanium isopropoxide was dissolved in the above 2-MOE-acetylacetone solution and was then stirred for 1.5 h. The titanium solution was added to the Bi-La-Fe solutions with continuous stirring at room temperature, and the final mixture was stirred for an additional 2 h. The concentrations of all solutions were calculated to 0.1 M.

All the thin films were deposited on $Pt(111)/Ti/SiO_2/Si(100)$ substrates by using a spin coating method at a constant spinning rate of 3000 rpm for 20 s. The coated wet films were prebaked sequentially at 200 °C and 360 °C for 5 min on a hot plate. The coating and the prebaking processes were repeated for 15 times to obtain the desired film thickness. Finally, all the thin films were subjected to rapid thermal annealing at 650 °C for 3 min under an oxygen atmosphere for crystallization. The platinum electrodes with areas of 1.54×10^{-4} cm^2 were deposited on the top surfaces of the thin films by ion sputtering through a shadow metal mask to measure the electrical properties.

The structures of the thin films were analyzed by using an X-ray diffractometer (Rigaku, MiniFlex II) and a Raman spectroscope (Jasco, NRS-3100). The surface morphologies and the microstructural features were examined by using a field emission scanning electron microscope (Tescan, MIRA II LMH). The leakage current densities of the thin films were measured by using an electrometer (Keithley, 6517A). The ferroelectric hysteresis loops of the thin films were traced at a frequency of 1.25 kHz by using a standardized ferroelectric test system (Radiant Technologies Inc., Precision LC). The dielectric properties were analyzed by using a low frequency impedance analyzer (HP, 4192A). The room temperature magnetic properties of the thin films were measured by using a physical property measurement system (Quantum Design Inc., PPMS-7).

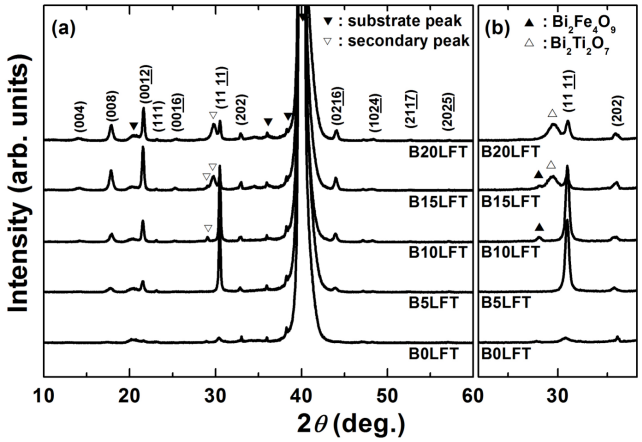

Fig. 1. XRD patterns of the B0LFT, B5LFT, B10LFT, B15LFT and B20LFT thin films deposited on Pt(111)/Ti/SiO_2/Si(100) substrates. (a) Magnified XRD patterns to show the secondary phase formation.

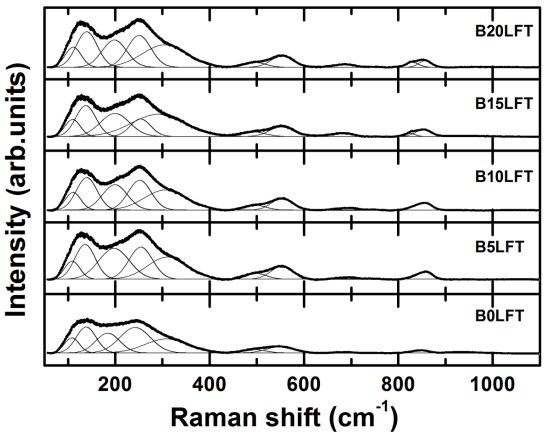

Fig. 2. Raman scattering spectra with fitted curves (thick solid lines) and the decomposed active modes (thin solid lines) of the B0LFT, B5LFT, B10LFT, B15LFT and B20LFT thin films measured at room temperature.

III. RESULTS AND DISCUSSION

The X-ray diffraction (XRD) patterns of the thin films prepared on Pt(111)/Ti/SiO_2/Si(100) substrates are shown in Fig. 1. X-rays with $CuK_{\alpha 1}$ radiation of wavelength $\lambda = 1.5418$ Å were used to observe the diffraction patterns. From Fig. 1(a), all the thin films were indexed with reference to the polycrystalline orthorhombic BLSFs structure [JCPDS No: 210101]. From Fig. 1(a), there were no secondary or impurity phases found for the B0LFT and the B5LFT thin films. The increase of Bi ion concentration above 5% leads to the formation of secondary phases, which have been clearly observed for the B10LFT, B15LFT and B20LFT thin films (Fig. 1(b)). These results imply that up to 5% the excessive Bi^{3+} ion concentration don't reach the solubility limit of the parent compound to commence the impurity phase. From XRD patterns, the B0LFT thin film showed relatively poor crystallization compared to the other thin films. It is important to note, the B5LFT and the B10LFT thin films showed relatively the low *c*-axis orientation and the dominant diffraction were found along $(11\bar{1})$ planes. The more *c*-axis orientation in the BLSFs could cause less ferroelectric polarization [6].

Figure 2 shows Raman scattering spectra of the thin films measured at room temperature. The exact peak positions have been estimated by fitting the measured spectra and decomposing the fitted curves into individual Lorentz components. In general, there are two sets of modes, such as low frequency modes (below 200 cm^{-1}) related to the *A*-site ions and the high frequency modes (above 200 cm^{-1}) related to the BO_6 octahedra of the BLSF's structures [5]. All of the Raman active modes observed for the thin films were assigned with reference to the BLSFs compounds, having similar structures [5, 24, 25]. The Raman peaks corresponding to the υ_1 and the υ_2 modes are attributed to the vibration of the Bi ion at the *A*-site of the pseudo-perovskite blocks [5,24]. The $\upsilon_{3,4,5,7}$ and υ_{10} active modes are related to the internal vibrational modes of the TiO_6 octahedra [5,25]. The υ_6 and υ_8 modes correspond to the FeO_6 vibrational modes [24]. The υ_9* mode observed for the B15LFT and the B20LFT may be due to the impurity phase. From the Raman scattering spectra, the peaks are broadened in the low frequency region, which might be attributed to the La doping into the Bi site of the $Bi_6Fe_2Ti_3O_{18}$. The La-O bond energy (798 kJ/mole) is larger than that of the Bi-O bond energy (343 kJ/mole), hence, the La ion incorporation into the Bi-site leads to dispersion of the Bi-O bond in the BLSFs structure. The dispersion of the Bi-O bond might be attributed to the peak broadening and the overlap of the peaks at low frequency region [26]. The observed Raman modes for the B0LFT, B5LFT, B10LFT, B15LFT and B20LFT are given in Table 1. Thus, both the Raman and the XRD studies confirm the formations of bismuth layer-structured compounds.

Figure 3 shows the surface morphologies of the thin films. For the B0LFT thin film, the surface morphology showed poorly crystallized grains with large pores

Table 1. Assignments of the Raman active modes for the B0LFT, B5LFT, B10LFT, B15LFT and B20LFT thin films.

Samples	Raman modes (cm^{-1})									
	$\upsilon 1$	$\upsilon 2$	$\upsilon 3$	$\upsilon 4$	$\upsilon 5$	$\upsilon 6$	$\upsilon 7$	$\upsilon 8$	$\upsilon 9*$	$\upsilon 10$
B20LFT	110.9	139.7	198.2	250.7	304.5	496.2	553.9	684.9	829.7	856.6
B15LFT	109.8	137.7	199.4	253.5	291.1	492.7	553.6	678.6	825.3	853.6
B10LFT	110.7	139.7	199.4	251.9	306.1	497.3	553.5	685.1	-	852.1
B5LFT	108.8	136.3	197.5	254.3	310.5	497.9	553.1	690.2	-	854.5
B0LFT	108.2	138.4	184.1	242.1	308.6	494.6	550.1	691.4	-	846.6

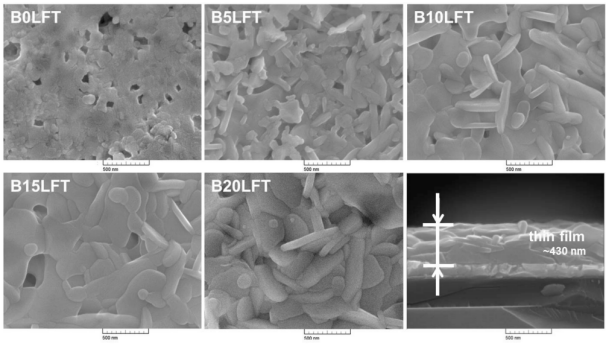

Fig. 3. SEM morphologies of the B0LFT, B5LFT, B10LFT, B15LFT and B20LFT thin films and cross-sectional micrograph of the B5LFT thin film.

between grains. The microstructures were changed as platelets like morphologies for the B5LFT, B10LFT, B15LFT and B20LFT thin films. The formation of the platelet like morphologies is the characteristics of the Aurivillius type layered structures [1]. The size of the platelet was increased for the B10LFT, B15LFT and B20LFT thin films. The thickness of the each thin film was estimated to be approximately 430 nm from the cross sectional SEM images.

In BLSF materials, oxygen vacancies are unavoidably formed due to the volatilization of bismuth during the material processing, such as prebaking and annealing. Experiment and theoretical studies have suggested that oxygen vacancies act as free carriers for the conduction [20]. Furthermore, the fluorite like $(Bi_2O_2)^{2+}$ layers play a significant role in the insulating properties of the BLSFs. ^{14}Bi volatilization leads to the structural instability in the bismuth layer structured compounds, which in turn degrades the electrical properties of the BLSF thin films. The variations of leakage current densities (J) with applied electric fields (E) for the thin films are shown in Fig. 4(a). From the leakage current analysis, the leakage current densities of the Bi excess BLFT

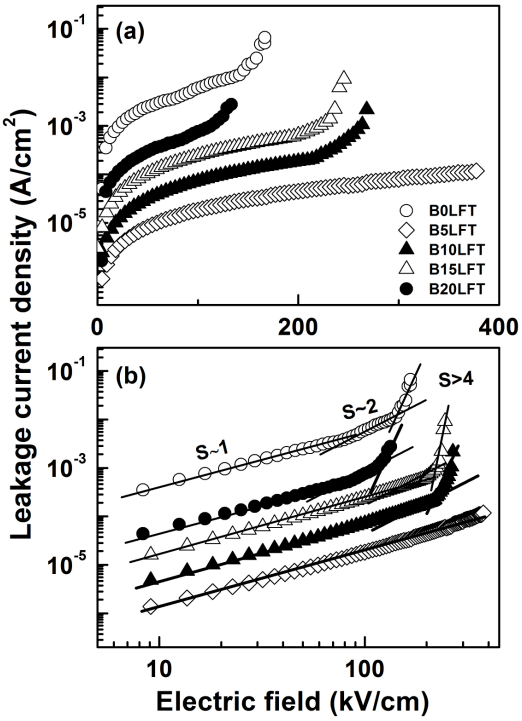

Fig. 4. (a) Leakage current densities of the B0LFT, B5LFT, B10LFT, B15LFT and B20LFT thin films and (b) $\log(J)$-$\log(E)$ characteristics of the thin films.

thin films were lower than that of the B0LFT thin film. The measured leakage current densities of the B0LFT, B5LFT, B10LFT, B15LFT and B20LFT thin films were 6.03×10^{-3}, 1.84×10^{-5}, 7.22×10^{-5}, 2.41×10^{-4} and 7.62×10^{-4} A/cm^2 at an electric field of 100 kV/cm, respectively. The large leakage current density of the B0LFT thin film could be attributed to the oxygen vacancies, poor crystallization, and porous microstructure [27]. The leakage current density of the B5LFT was three orders lower than that of the B0LFT thin film. Addition of excessive Bi leads to the compensation of Bi volatilization and stabilizes the BLSFs structure. The structure stabilization and the dense microstructure might be attributed to the low leakage current density of the B5LFT

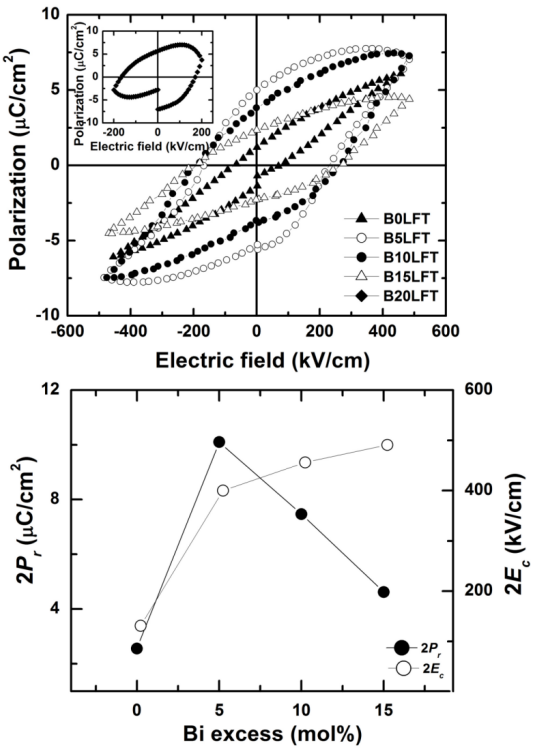

Fig. 5. (a) Ferroelectric $P-E$ hysteresis loops of the B0LFT, B5LFT, B10LFT, B15LFT and B20LFT thin films. (b) Variations of $2P_r$ and $2E_c$ with respect to the excessive Bi concentrations.

thin film. On the other hand, the B10LFT, B15LFT and B20LFT thin films attain easy electrical break down and exhibit relatively large electrical leakage current compared to the B5LFT thin film. The easy electrical break down of the B10LFT, B15LFT and B20LFT thin films is attributed to the formation of secondary phases. The secondary phases of the B10LFT, B15LFT and B20LFT thin films were clearly observed in the XRD patterns.

In order to understand the origin of the electrical leakage of the thin films, the conduction mechanisms was investigated by plotting log (J) versus log (E) as shown in Fig. 4(b). From Fig. 4(b), the linearity of the fitted line over the entire region of the applied electric field for the B5LFT thin film with slope value ∼1 indicates Ohmic conduction mechanism, which is dominated by thermally stimulated free electrons [28]. Leakage current for Ohmic conduction can be expressed as

$$J = e\mu N_e E,$$

where e is the electron charge, μ is the free carrier mobility, N_e is the density of the thermally stimulated electrons, and E is the applied electric field [28]. The plots can be fitted well by linear segments with different slope values for the B0LFT, B10LFT, B15LFT, and B20LFT thin films. The B0LFT, B10LFT, B15LFT and B20LFT thin films showed Ohmic conduction upto certain applied electric field with slope value ∼1. However, the change of slope value from ∼1 to ∼2 with increase of applied electric field implies the change of conduction mechanism from Ohomic to space charge limited (SCL) conduction [28]. In the SCL conduction process, the density of free electrons due to carrier injection becomes larger than the density of thermally stimulated electrons [28]. The current density for SCL conduction is given by

$$J_{SCL} = (\frac{9\mu\varepsilon_0\varepsilon_r\theta}{8}\frac{V_2}{d^3}),$$

where V is the applied voltage, ε_r is the static dielectric constant, ε_0 is the permittivity of free space, d is the thickness of thin film, and θ is the ratio of the total density of free electrons to the trapped electrons [28]. On further increasing applied electric field, an abrupt increase of leakage current with the slope value greater than 4 was observed. The slope value greater than 4 indicates the trap filled limited (TFL) conduction mechanism [28]. In the high electric field region, the excess charge careers remain after filling all available traps by the applied electric field, which in turn lead drastic increase of the current with large slope value. The voltage at which abrupt increase of the current occurs is TFL voltage and given by

$$V_{TFL} = \frac{eN_t d^2}{2\varepsilon_0\varepsilon_r},$$

where N_t is the total trap density [28]. Thus, the leakage occurred in the B0LFT, B10LFT, B15LFT and B20LFT thin films were originated from the Ohmic, SCL and TFL conduction mechanisms. The conduction observed in the B5LFT thin film was originated from the Ohmic conduction mechanism.

As it is well known, the values of remnant polarization and coercive electric field of ferroelectric thin film have been affected by various factors, such as domain pinning, ionic displacement, orientation, *etc.* [20,29]. The polarization-electric field ($P-E$) hysteresis loops of the thin films measured at 1.25 kHz are shown in Fig. 5(a). Variations of the $2P_r$ and the $2E_c$ with respect to the excessive Bi concentration are shown in Fig. 5(b). Among

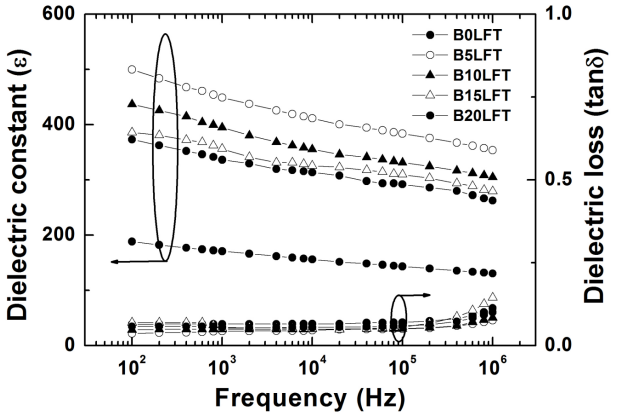

Fig. 6. Frequency dependent dielectric properties of the B0LFT, B5LFT, B10LFT and B20LFT thin films.

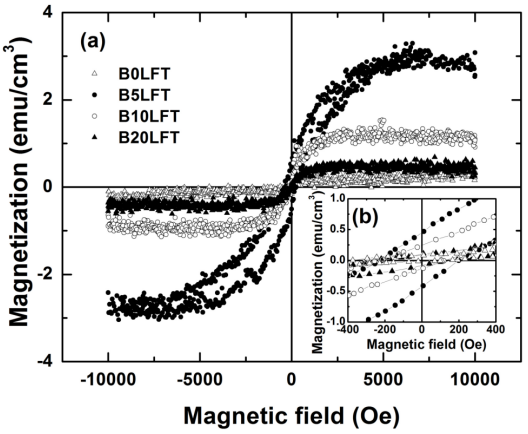

Fig. 7. Magnetization-magnetic field ($M-H$) hysteresis loops of the B0LFT, B5LFT, B10LFT and B20LFT thin films measured at room temperature.

the thin films, the B5LFT thin film showed a large remnant polarization and a low coercive filed, which are well correlated with the small leakage current density of the B5LFT thin film. The remnant polarization ($2P_r$) and the coercive field ($2E_c$) values of the B0LFT, B5LFT, B10LFT and B15LFT thin films were 2.4 μC/cm^2 and 131 kV/cm at 458 kV/cm, 10.5 μC/cm^2 and 400 kV/cm, 7.5 μC/cm^2 and 456 kV/cm and 4.6 μC/cm^2 and 491 kV/cm at an electric field of 485 kV/cm, respectively. The values of the remnant polarization were well correlated with the leakage current densities of the thin films. Poor crystallization and large leakage current lead to the small remnant polarization and the low electrical breakdown voltage of the B0LFT thin film. Formation of stable layer-structured phase with reduced oxygen vacancies and small leakage current are correlated to the improved ferroelectric properties of the B5LFT thin film. As shown in inset, the secondary phases lead to leaky hysteresis loop for the B20LFT. Furthermore, the orientation of thin film also influences on the ferroelectric polarization [6,29]. As it can be seen in the XRD analysis, the B5LFT and the B10LFT thin films exhibited relatively less *c*-axis orientation compared to the other thin films and showed large remnant polarization [29].

Frequency dependent dielectric properties of the B0LFT, B5LFT, B10LFT and B20LFT thin films were measured at room temperature by varying applied frequencies from 10^2 to 10^7 Hz as shown in Fig. 6. The measured dielectric constant (ε) values of the B0LFT, B5LFT, B10LFT and B20LFT thin films were 171, 449, 395 and 336, respectively, at an applied frequency of 1 kHz. At the same applied frequency, the measured dielectric loss values of the B0LFT, B5LFT, B10LFT and B20LFT thin films were 0.06, 0.04, 0.05 and 0.06, respectively. The porous microstructure may be attributed low dielectric constant and high dielectric loss of the B0LFT thin film.

The magnetic structure of the $Bi_6Fe_2Ti_3O_{18}$ was explained by the existence of the antiferromagnetic interaction with the dominant paramagnetic state. The antiferromagnetism was correlated with the superexchange interaction among Fe^{3+}-O-Fe^{3+} bond [13]. We have investigated the magnetic properties of the thin films at room temperature. Interestingly, weak ferromagnetic properties were observed at room temperature for the B0LFT, B5LFT, B10LFT and B20LFT thin films. The observed weak ferromagnetism might be attributed to the structural distortion caused by the La incorporation into the Bi-site of the $Bi_6Fe_2Ti_3O_{18}$ [22]. The rare earth La ion doping into the $Bi_6Fe_2Ti_3O_{18}$ can able to tilt the [FeO6] octahedra and the latent magnetization locked in the antiferromagnetic state might be released [22]. Additionally, the local ferromagnetic Fe-O clusters and the existence of Fe^{2+} ions caused by the oxygen vacancies might also contribute to the weak ferromagnetic behavior [21, 30, 31]. The saturated magnetization-magnetic field ($M-H$) hysteresis loops for the B0LFT, B5LFT, B10LFT and B20LFT thin films are shown in Fig. 7(a). All the thin films exhibited a weak ferromagnetism with the saturation at 10 kOe. From the Fig. 7(b), the calculated remnant magnetization ($2M_r$) and the coercive

magnetic field ($2H_c$) for the B0LFT, B5LFT, B10LFT and B20LFT thin films were 0.10 emu/cm^3 and 0.56 kOe, 0.90 emu/cm^3 and 0.41 kOe, 0.34 emu/cm^3 and 0.37 kOe and 0.16 emu/cm^3 and 0.47 kOe, respectively, at an applied magnetic field of 10 kOe. The better ferromagnetism observed in the B5LFT thin film might be attributed to the formation of the stable bismuth layer-structured compound and the structural distortion [30].

IV. CONCLUSIONS

Aurivillius La-doped $Bi_6Fe_2Ti_3O_{18}$ ($Bi_{5.25}La_{0.75}Fe_2Ti_3O_{18}$) thin films with various excessive Bi concentrations (0, 5, 10, 15 and 20% denoted by B0LFT, B5LFT, B10LFT, B15LFT and B20LFT) were prepared on Pt(111)/Ti/SiO_2/Si(100) substrates by a chemical solution deposition method. From X-ray diffraction analysis, the formation of secondary phase was clearly observed for the thin films having more than 5% of the excessive Bi concentration. Among the thin films, the B5LFT thin film showed superior electrical, ferroelectric, and ferromagnetic properties. The leakage current density of the B5LFT thin film was three orders higher than that of the B0LFT thin film. The $2P_r$ and $2E_c$ values of the B5LFT thin film were 10.5 μC/cm^2 and 400 kV/cm at an electric field of 485 kV/cm, respectively. The improved properties were correlated to the compensation of the Bi volatilization in the La-doped $Bi_6Fe_2Ti_3O_{18}$ thin film by the addition of excessive Bi ion, which in turn controls the oxygen vacancies and stabilizes the bismuth layer structured phase. All thin films showed a weak ferromagnetic property, which might be attributed to the structural distortion caused by the doping of La ion into the $Bi_6Fe_2Ti_3O_{18}$ compound.

ACKNOWLEDGEMENTS

This research is financially supported by Changwon National University in 2013∼2014.

REFERENCES

[1] L. Keeney, P. F. Zhang, C. Groh, M. E. Pemble and R. W. Whatmore, J. Appl. Phys. **108**, 042004 (2010).
[2] J. F. Scott, Science **315**, 954 (2006).
[3] H. Watanabe, T. Mihara, H. Yoshimori and C. A-Paz de Araujo, Jpn. J. Appl. Phys. **34**, 5240 (1995).
[4] T. Watanabe and H. Funakubo, J. Appl. Phys. **100**, 051602 (2006).
[5] S. Kojima, R. Imaizumi, S. Hamazaki and M. Takashige, Jpn. J. Appl. Phys. **33**, 5559 (1994).
[6] H. Irie, M. Miyayama and T. Kudo, J. Appl. Phys. **90**, 4089 (2001).
[7] S. K. Patri, R. N. P. Choudhary and B. K. Samantaray, J. Electroceram. **20**, 119 (2008).
[8] A. Srinivas, S. V. Suryanarayana, G. S. Kumar and M Mahesh Kumar, J. Phys.: Condens. Matter **11**, 3335 (1999).
[9] M. I. Morozov and V. V. Gusarov, Inorg. Mater. **38**, 723 (2002).
[10] X. Y. Mao, W. Wang and X. B. Chen, Solid State Commun. **147**, 186 (2008).
[11] J. Yang, L. H. Yin, Z. Liu, X. B. Zhu and W. H. Song *et al.*, Appl. Phys. Lett. **101**, 012402 (2012).
[12] W. Bai, Y. Q. Gao, J. Y. Zhu, X. J. Meng and T. Lin *et al.*, J. Appl. Phys. **109**, 064901 (2011).
[13] J. Yang, W. Tong, Z. Liu, X. B. Zhu and J. M. Dai *et al.*, Phys. Rev. B **86**, 104410 (2012).
[14] F. Huang, X. Lu, T. T. Xu, Y. Liu and W. Su *et al.*, Thin Solid Films **520**, 6489 (2012).
[15] J. -A. Deverin, Ferroelectrics **19**, 9 (1978).
[16] J. Lu, L. J. Qiao, X. Q Ma and W. Y. Chu, J. Phys.: Condens. Matter **18**, 4801 (2006).
[17] Z. Liu, J. Yang, X. W. Tang, L. H. Yin and X. B. Zhu *et al.*, Appl. Phys. Lett. **101**, 122402 (2012).
[18] J. -B. Li, Y. P. Huang, G. H. Rao, G. Y. Liu and J. Luo *et al.*, Appl. Phys. Lett. **96**, 222903 (2010).
[19] L. Keeney, C. Groh, S. Kulkarni, S. Roy and M. E. Pemble *et al.*, J. Appl. Phys. **112**, 024101 (2012).
[20] H. Sun, J. Zhu, H. Fang and X. Chen, J. Appl. Phys. **100**, 074102 (2006).
[21] S. Y. Lee, C. W. Ahn, H. J. Lee, S. H. Kang and J. S. Kim *et al.*, J. Korean Phys. Soc. **46**, 337 (2005).

[22] F. Huang, X. Lu, C. Chen, W. Lin and X. Chen *et al.*, Solid State Commun. **150**, 1646 (2010).

[23] H. Sun, X. Lu, J. Su, T. Xu and C. Ju *et al.*, J. Phys. D: Appl. Phys. **45**, 385001 (2012)

[24] X. Mao, H. Sun, W. Wang, Y. Lu and X. Chen, Solid State Commun. **152**, 483 (2012).

[25] J. Wang, G. X. Cheng, S. T. Zhang, H. W. Cheng and Y. F. Chen, Physica B **344**, 368 (2004).

[26] Z. Hu, M. Li, Y. Yu, J. Liu and L. Pei *et al.*, Solid State Commun. **150**, 1088 (2010).

[27] D. Do, S. S. Kim, T. K. Song and B. C. Choi, J. Korean Phys. Soc. **55**, 613 (2009).

[28] C. Wang, M. Takahashi, H. Fujino, X. Zhao and E. Kume *et al.*, J. Appl. Phys. **99**, 054104 (2006).

[29] M. Miyayama and I. -S. Yi, Ceram. Int. **26**, 529 (2000).

[30] N. V. Prasad and G. S. Kumar, J. Magn. Magn. Mater. **213**, 349-56 (2000).

[31] H. Sun, X. Lu, T. Xu, J. Su and Y. Jin *et al.*, J. Appl. Phys. **111**, 124116 (2012).